Acta Materialia 131 (2017) 123–130

Contents lists available at ScienceDirect

Acta Materialia

journal homepage: www.elsevier.com/locate/actamat

Full length article

Thickness-dependent a_1/a_2 domain evolution in ferroelectric $PbTiO_3$ films

S. Li [a, b], Y.L. Zhu [a, *], Y.L. Tang [a], Y. Liu [a], S.R. Zhang [a, b], Y.J. Wang [a], X.L. Ma [a, c]

[a] Shenyang National Laboratory for Materials Science, Institute of Metal Research, Chinese Academy of Sciences, Wenhua Road 72, 110016 Shenyang, China
[b] University of Chinese Academy of Sciences, Yuquan Road 19, 100039 Beijing, China
[c] School of Materials Science and Engineering, Lanzhou University of Technology, Langongping Road 287, 730050 Lanzhou, China

ARTICLE INFO

Article history:
Received 18 January 2017
Received in revised form
22 March 2017
Accepted 25 March 2017
Available online 27 March 2017

Keywords:
Ferroelectric
$PbTiO_3$
a_1/a_2 domain structure
Transmission electron microscopy

ABSTRACT

Ferroelectric a_1/a_2 domain structure has great potentials in high dielectric capacitors and tunable microwave devices. Understanding its structure is crucial to better control the domain configurations for future applications. In this paper, $PbTiO_3$ thin films with variant thicknesses are deposited on (110)-oriented $GdScO_3$ substrates by Pulsed Laser Deposition (PLD) and investigated by using conventional transmission electron microscopy (TEM) and Cs-corrected Scanning TEM. Contrast analysis and electron diffractions reveal that $PbTiO_3$ films are domain oriented consisting of a_1/a_2 and a/c domain structure. The a_1/a_2 domains are found to distribute periodically and its width increases with increasing film thickness following square root rule. Cs-corrected STEM imaging demonstrates that the domain walls of a_1/a_2 domain structure have the rotation characteristic of 90° ferroelastic domain wall. The interchange of a_1/a_2 domains induces the formation of vertex domains composed of two 90° and one 180° domain walls. Strains are mainly concentrated on the domain walls. The formation of this complex domain configuration is discussed in terms of the effect of the misfit strain, film thickness and cooling rate. These results provide novel information about a_1/a_2 domain structures and are expected to shed some light on modulating a_1/a_2 ferroelectric domain patterns in the design of ferroelectric-based devices.

1. Introduction

Ferroelectric films have attracted increasing interest for various applications including nonvolatile ferroelectric random access memory devices (FeRAM) due to their spontaneous ferroelectric polarization [1,2]. It is especially important to understand the domain formation rules to control domain structure since it has a profound influence on ferroelectric and piezoelectric properties of ferroelectric films.

In tetragonal ferroelectric film, according to the different *c*-axis orientations, ferroelectric domains are generally classified into three domain types: *c*-domain with the *c*-axis normal to the film/substrate interface and two types of *a*-domains with the *c*-axis along [100] or [010] direction (two in-plane directions) [3–6]. The formation of domain structure is usually affected by film thickness, substrate mismatch strain, depolarizing field and cooling rate *etc.*, while the size of each domain changes with film thickness in order to balance the system energy such as electrostatic energy, elastic strain energy and the domain wall formation energy [4,7–10].

In the past a few years, much attention has been regenerated to the morphology of domain structure and some novel domain patterns have been observed or simulated, such as ferroelectric flux-closure quadrants, vortices and $c/a_1/a_2$ domain structure [4,11–13]. There are also theoretical works about how the domain structure and the width of domains change in ferroelectric films with varying temperature, misfit strain and film thickness [14–16]. Thermodynamic analysis and phase-field simulations indicate that the stable domain structure of $PbTiO_3$ (PTO) film evolves from *c* to $c/a_1/a_2$ and then to a_1/a_2 (or named a/a) in room temperature with the misfit strain changing from compressive to tensile [5,6,9,10,13,17–19]. This conclusion is also partly supported by some experimental evidences, for example, PTO films consist of a/c domain structure when grown on $DyScO_3$ substrate (small tensile stress) and become a/a domain structure on $SmScO_3$ substrate (large tensile stress) [7,20,21]. As to the effects from film thickness, some experimental results imply that film thickness affects not only domain size but also domain structure. It was reported that in systems with small lattice misfit, complex domain structures

* Corresponding author.
E-mail address: ylzhu@imr.ac.cn (Y.L. Zhu).

http://dx.doi.org/10.1016/j.actamat.2017.03.064
1359-6454/

consisting of c/a_1 and a_2/a_3 stripes were found in thick (2.8 μm) epitaxial (001)-oriented PTO films grown on Nb-doped $SrTiO_3$ substrates by piezoresponse force microscopy and high-resolution x-ray diffraction analysis [4,22]. It was proposed that these complex domain patterns formed only in the thick film due to the relaxation of residual strain, which made the film similar to bulk status. In contrast to the numerous investigations on typical a/c domains, a_1/a_2 domains are not well uncovered. Since a_1/a_2 domain structure is preferred to be applied in high dielectric capacitors and other related fields [20,23,24], it is important to study the evolution of a_1/a_2 domains with changing film thickness especially when the films are under large misfit strains. Besides, previous theoretical calculations about a_1/a_2 domain structure indicate that there is a quadratic dependence, $W \propto d^{1/2}$, of the domain width (W) with the film thickness (d) [23,25,26].

In this study, domain patterns especially the details of ferroelastic 90° a_1/a_2 domain structure in PTO films grown on (110)-oriented $GdScO_3$ (GSO) substrate are systematically studied. This substrate is chosen because it provides PTO film a large tensile strain at room temperature which can be relaxed by forming different domains without misfit dislocations during cooling process. In general, dislocation has a significant impact on domain structure formation and evolution, so this work eliminates the effects of misfit dislocations and creates a condition to study the correlation between domain structures and misfit strains only. The absence of defects also allows domains to form in a very periodic fashion [7,27]. Therefore, the thickness dependence of the periodic a_1/a_2 domain structure can be summarized and is verified to be fully compliant with the previous theoretical predictions.

2. Experiment

The PTO thin films were grown on (110)-oriented GSO substrates by Pulsed Laser Deposition (PLD), using a 248 nm KrF excimer laser. The PTO target was 3 mol% lead-enriched sintered ceramics. Before deposition, the GSO substrate was heated at 800 °C for 5 min and then kept at 700 °C. The PTO target was pre-ablated for 15 min to clean the surface. During the growth of the PTO film, an oxygen pressure of 20 Pa, a laser energy density of 2 Jcm^{-2} and a repetition rate of 2 Hz were used. After deposition, the film was stabilized at 700 °C for 5 min and then cooled down to room temperature at 5 °C min^{-1} in an oxygen pressure of 3×10^4 Pa. Cross-sectional and plan-view samples were prepared by slicing, grinding, dimpling and finally ion milling by using Gatan PIPS, while plan-view samples were milled only from the substrate side. The final ion milling voltage was less than 0.5 kV to reduce amorphous layer produced by ion beam damage. A JEOL 2100 transmission electron microscope was used for electron diffraction and diffraction contrast analysis. The HAADF-STEM image was acquired using a Titan G^2 60–300 microscope with a high-brightness field-emission gun and double aberration (Cs) correctors from CEOS operating at 300 kV, while the beam convergence angle was 25 mrad and the collection angle ranged from 50 mrad to 250 mrad. The Fast Fourier Transformed (FFT) patterns of the plan-view TEM images were used for the statistics of the average width of a_1/a_2 domain structure. Strain fields were deduced by using custom plugins of GPA for Gatan Digital Micrograph. The visualizations of the strains and lattice rotations were carried out using Gatan Digital Micrograph software.

3. Results

For simplicity, orthorhombic (110)-GSO substrates are treated as (001) orientation of pseudo cubic (pc) perovskite in the present study. All the orientations marked below without subscripts represent pseudo cubic perovskite and [001] orientation indicates the out-of-plane direction which is the direction of film growth. Fig. 1 shows the cross-sectional bright field TEM images of PTO films with different thicknesses grown on GSO substrate. From Fig. 1(a), it can be seen that the interface of film/substrate is flat as denoted by a pair of arrows. The thickness of the film is around 22 nm. Some stripe-like areas showing bright and dark contrast are observed in the film. They distribute nearly periodically in the film with the width (W) of about 26 nm. It is seen that these contrasts are approximately perpendicular to the interface. Increasing film thickness from 22 nm to 43 nm, 54 nm and finally 86 nm, the morphologies of the films are shown in Fig. 1(b–d). It is noted that with increasing the film thickness, the widths of stripe-like areas increase accordingly. It is also observed that besides the areas mentioned above in Fig. 1(a), some stripes appear in the films forming about 45° angle with the interfaces, which are believed to be typical a/c domains commonly in ferroelectric films [7,27,28]. These ordinary a/c domain structure has domain walls lying on (011) or $(0\bar{1}\ 1)$ plane from cross-sectional observations. Usually, the stripes-like contrast normal to the interfaces may come from 180° stripe domain, a_1/a_2 domains, threading dislocations or other planar defects like stacking faults. Some calculation work indicated that a-domain is easy to form under large tension strains and may turn into a_1/a_2 domain structure [20]. Considering the polarization direction of a-domain along [100] or [010] direction and the strong correlation between polarization and lattice, the domain wall of a_1/a_2 domain structure is determined to be along (110) or $(1\bar{1}\ 0)$ plane. When observed approximately along [100] direction, the projections of a_1/a_2 domain walls should be normal to the interface and present fuzzy areas instead of sharp lines because the projection direction is not parallel to the domain wall. The stripe-like contrast normal to the interfaces shown in Fig. 1 might be from a_1/a_2 domain structure, although the possibility of other defects mentioned above could not be excluded only by the bright-field images.

To accurately distinguish them, electron diffraction experiments are performed on cross-sectional TEM samples which is a powerful tool to determine the phase structures. Selected area electron diffraction (SAED) patterns taken from different areas including both the films and the substrates are shown in Fig. 2. Fig. 2(a) is an SAED pattern taken from the area including the substrate, a/c domains and a_1/a_2 domains in 54 nm thick PTO film on GSO substrate. The diffraction pattern is complex especially with high-index spots. Fig. 2(b) and (c) are the enlargement of out-of-plane (002) reflection (labeled as 1) and in-plane (020) reflection (labeled as 2) in Fig. 2(a), respectively. The circular reflection peaks at the center of Fig. 2(b) and (c) are indexed as 002s and 020s of the GSO substrate. The subscript 's' denotes substrate. As shown in Fig. 2(b), the diffraction spot marked by 002a represents a-domain whose out-of-plane lattice constant is about 0.39 nm, smaller than GSO and close to the a-axis lattice constant of PTO bulk (a = 0.389 nm, c = 0.414 nm) [29]. The two spots labeled as 002c represent two kinds of c-domains differed by a small angle which may relate to the a/c domain structures that have different domain walls along (011) and $(0\bar{1}\ 1)$ plane. Generally, there should be two 002a split spots in Fig. 2(b) corresponding to two 002c spots. The absence of one 002a spot is considered to be too weak to detect because this kind of a-domain has a small volume fraction in the selected area. In Fig. 2(c), spot marked with 020a comes from a-domain whose c-axis along [010] direction just corresponding to 002a in Fig. 2(b). Based on the observation of $(0\bar{2}\ \bar{2}\ )$ reflection splitting into three spots in Fig. 2(a), it is easy to deduct that the big ellipse spot in Fig. 2(c) actually contains three spots. Two of them are indexed as 020c, the same as 002c in Fig. 2(b). The third one is supposed to come from the stripe domains with line contrasts normal to interface and it is indexed as $020a_2$ according to the calculation of

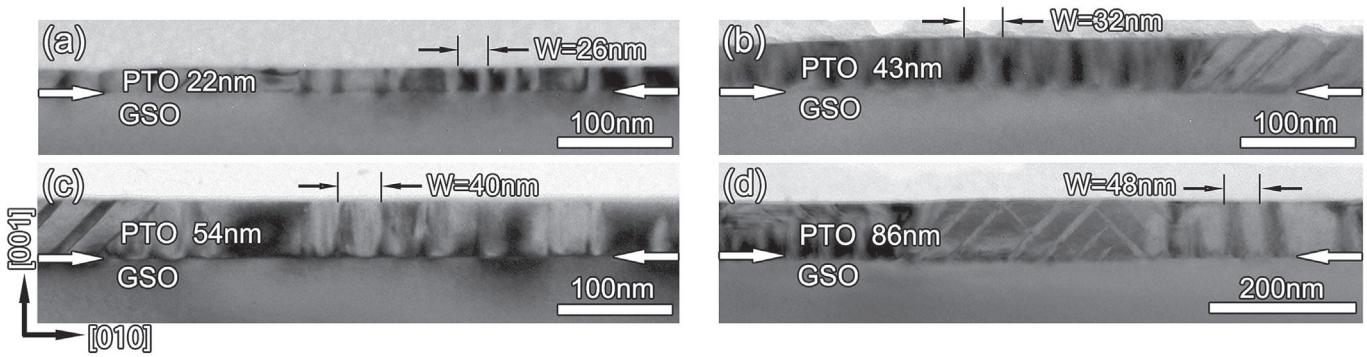

Fig. 1. Cross-sectional bright field TEM images of PTO films with different thicknesses grown on GSO $(110)_o$ substrate. (a) 22 nm; (b) 43 nm; (c) 54 nm; (d) 86 nm. The interface is marked by a pair of white arrows. *W* represents the width of a_1/a_2 domain structure.

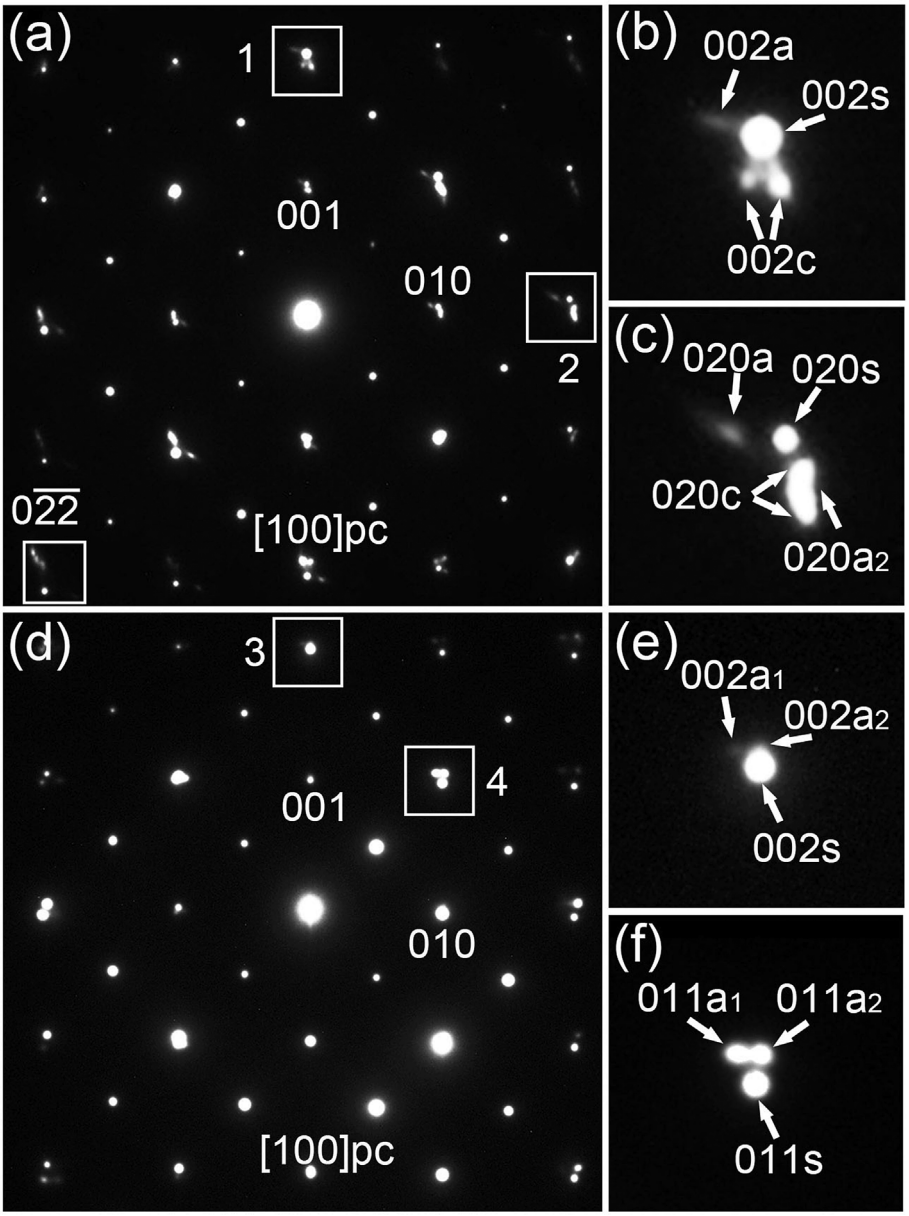

Fig. 2. Selected area electron diffraction (SAED) patterns of PTO films on GSO substrate. (a) SAED pattern taken from the area including the substrate, a_1/a_2 and *a*/*c* domains; (b) and (c) are the enlargements of rectangles labeled as 1 and 2 in (a). (d) SAED pattern taken from the area including the substrate and a_1/a_2 domains only. (e) and (f) are the enlargement of rectangles labeled as 3 and 4 in (d), respectively.

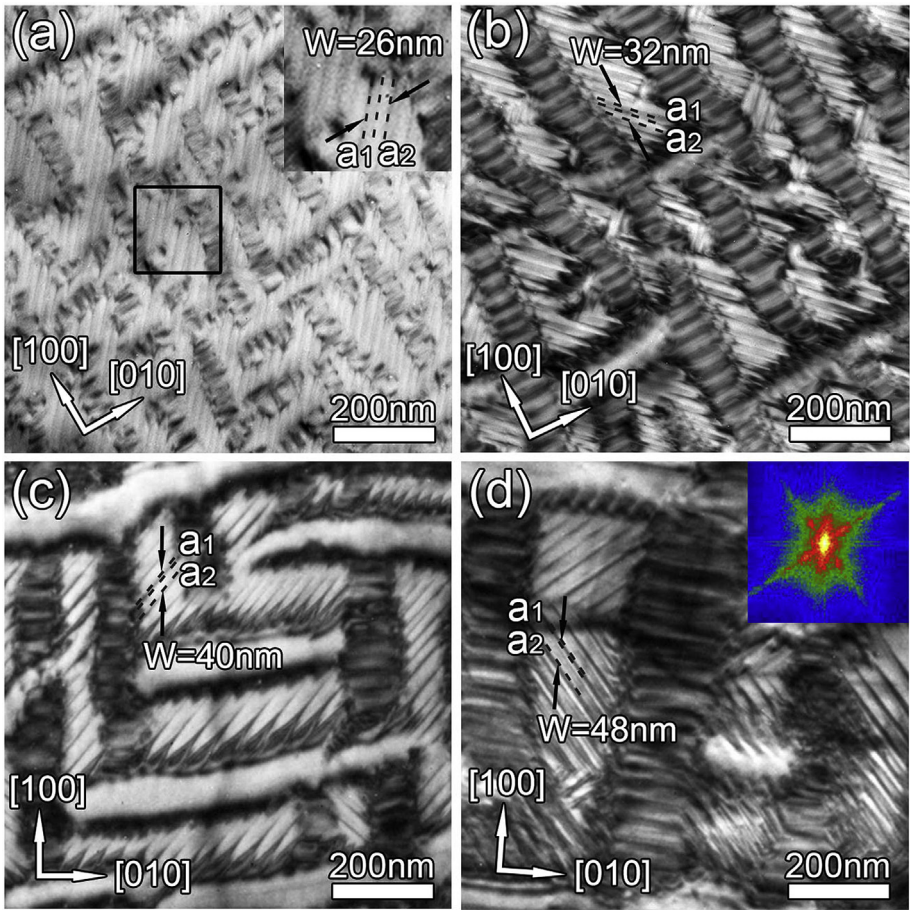

Fig. 3. Plan-view TEM images recorded from (a) 22 nm (b) 43 nm (c) 54 nm (d) 86 nm PTO films on GSO substrate. The a_1/a_2 domain structure is marked by a pair of black arrows. The inset shows the Fast Fourier Transform pattern of (d).

a-axis lattice constants along [010] and [001] directions. This result implies that these stripe domains may contain one kind of *a*-domain whose *c*-axis along [100] direction. It is noteworthy that $(0\bar{2}\,\bar{2}\,)$ spot consists of four spots, in which the strong one is from GSO. Besides two spots from *a*/*c* domains, the rest should be from *a*/*a* domains. To verify this, SAED pattern was taken from the area including the substrate and a_1/a_2 domains only, as shown in Fig. 2(d). Fig. 2(e) and (f) are the enlargement of out-of-plane (002) reflection (marked with 3) and (011) reflection (marked with 4) in Fig. 2(d). The (011) reflection is chosen instead of (020) reflection because the spot splitting can be clearly identified. In Fig. 2(f), the strong spot is indexed as 011s of GSO, while the weak two spots are indexed as $011a_1$ and $011a_2$, matching well with lattice constants of a_1 and a_2 domains along [010] direction of 0.413 nm and 0.391 nm, respectively. The (002) reflection in Fig. 2(e) does not show clear splitting but displays a slight elongation along the out-of-plane direction which indicates the lattice constant along [001] direction is smaller than that of GSO. Combining the diffraction analysis above, besides typical *a*/*c* domains, the stripe domain structure are determined to consist of two kinds of *a*-domains whose *c*-axis along [010] and [100] direction, respectively. In addition, the *a*/*c* and a_1/a_2 domains show different misorientation angles. The angle is calculated to be 3.6° for *a*/*c* domains in PTO considering its bulk lattice constants [27,28]. The angle measured from Fig. 2(a) is fitting well with the value; while the angle of a_1/a_2 domains is calculated to be 1.8° based on different interplanar spacings of a_1 and a_2 domains. The value measured from split spots near (011) reflection in Fig. 2(d) is about 1.5°, a slight smaller than expected. The angle of a_1/a_2 domain structure will be discussed in details later.

As shown in Fig. 1, the a_1/a_2 domain structure is periodic as $a_1/a_2/a_1/a_2$ … arrangement. The width of (a_1+a_2) repeating unit measured on different thick PTO films shows a positive correlation with the film thickness. However, it is difficult to judge the relationships of the volume fraction of a_1/a_2 domain structure with the film thickness because of limited observation area in cross-sectional sample. In order to further study the a_1/a_2 domain structure and its distribution regularities, plan-view BF-TEM images of PTO films with each thickness were taken and displayed in Fig. 3. Comparing Figs. 1 and 3, it is easy to find that a_1/a_2 domain structure with domain walls along (110) and $(1\bar{1}\,0)$ distributes regularly with sharp wall contrast; while the domain walls of *a*/*c* domain structures along (101) and (011) planes are blurred which are parallel to [100] and [010] direction, respectively, when observed from plan-view observations. The proportion of a_1/a_2 domain structure is approximately equal to that of *a*/*c* domains and barely changed with the increment of the film thickness though the widths of a_1/a_2 domains increase. To maintain the consistency with the results from cross-sectional images, we measured the width of a_1/a_2 domain (*W*) along [100] or [010] direction instead of perpendicular distance along [110] or $[1\bar{1}\,0]$ direction, as indicated by the black arrows in Fig. 3. To realize the validity, we also calculate the distances from spots in the Fast Fourier Transform (FFT) patterns of the plan-view TEM images, one of which is shown in the inset of Fig. 3(d). This inset shows spots corresponding to the periodicity of a_1/a_2 domain. Note that the lengths obtained from FFT patterns by measuring the spot distance are the perpendicular

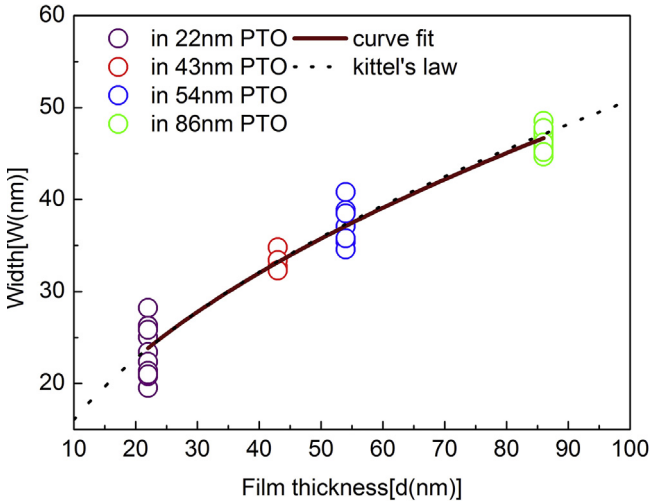

Fig. 4. The observed domain width (W) of periodic a_1/a_2 domains as a function of film thickness (d) for PTO thin films grown on GSO substrates. The curve fit is close to kittel's law ($W \propto d^{1/2}$).

distance along [110] or [1$\bar{1}$ 0] direction so the data are multiplied by square root of 2 to turn into the widths along [100] or [010] direction for consistency. The data collected from all the samples with different film thicknesses are summarized and shown in Fig. 4. The scatter of points is extracted based on the data obtained from the plan-view samples by the direct measurement in the images and counting through FFT patterns. The data was then fitted in two ways by using Origin software. One is $y = a + bx$ for the linear fit. The result is a = 16.2 and b = 0.36 with standard errors of 0.76 and 0.012, respectively. The other is $y = ax^b$ for the curve fit. The result is a = 4.9 and b = 0.5 with standard errors of 0.35 and 0.017, respectively. The curve fit shows relatively small standard errors and thus is more appropriate. As in Fig. 4, the red line is the curve fit to the experimental values displaying the relationship between the width of a_1/a_2 domain (W) and film thickness (d), which shows a good agreement with well established Kittel's law in ferroics marked by dashed line.

In order to clearly reveal the details of a_1/a_2 domain structure, high-resolution HAADF-STEM imaging was carried out. Fig. 5(a) is an HAADF-STEM image showing the intersections of two a_1/a_2 domain structures with different orientations in plan-view observations. The blue dashed lines trace the a_1/a_2 domain walls, while the red dashed lines trace the 180° domain walls. In tetragonal PTO film, the spontaneous polarization (Ps) projection is opposite to sub-lattice Ti displacement which can be used to determine the polarizations of each unit cell [11,28]. To identify the Ps direction of each domain area, atomic resolution HAADF-STEM image is given in Fig. 5(b), demonstrating the cation displacements in the area labeled with white rectangle in Fig. 5(a), where the yellow and red circles denote the positions of Pb and Ti atom columns, respectively. The intensity of atom columns is approximately proportional to the square of atomic number in HAADF-STEM image, so Pb atom columns is brighter than Ti which can be distinguished easily. By spotting the positions of Pb and Ti atom columns, reversed Ti atom displacement directions as well as the Ps directions of each domain area are thus determined and denoted by yellow arrows in Fig. 5(b). The Ps direction in Fig. 5(a) can be deduced easily after examining each area in Fig. 5(a) with the same procedure as performed on Fig. 5(b). It is noteworthy that two 90° domain walls and one 180° domain wall actually form a threefold vertex domain identified in Fig. 5(b). It is also noted that the misorientation angle of a_1/a_2 domains can be revealed as indicated by the purple and green line in Fig. 5(b). The insert in Fig. 5(b) is a schematic showing the lattice rotation with the angle of approximately 2.7° on two sides of the 90° a_1/a_2 domain wall. For better understanding of the strain distribution around a_1/a_2 domains, the in-plane strain (ε_{xx}) map by GPA analysis with the reciprocal lattice vector (100) and (010) is shown in Fig. 6(a). The line profiles performed from left to right along the routes labeled 1 and 2 are shown in Fig. 6(b) and (c), respectively. In Fig. 6(a), it is evident that the strain distribution is

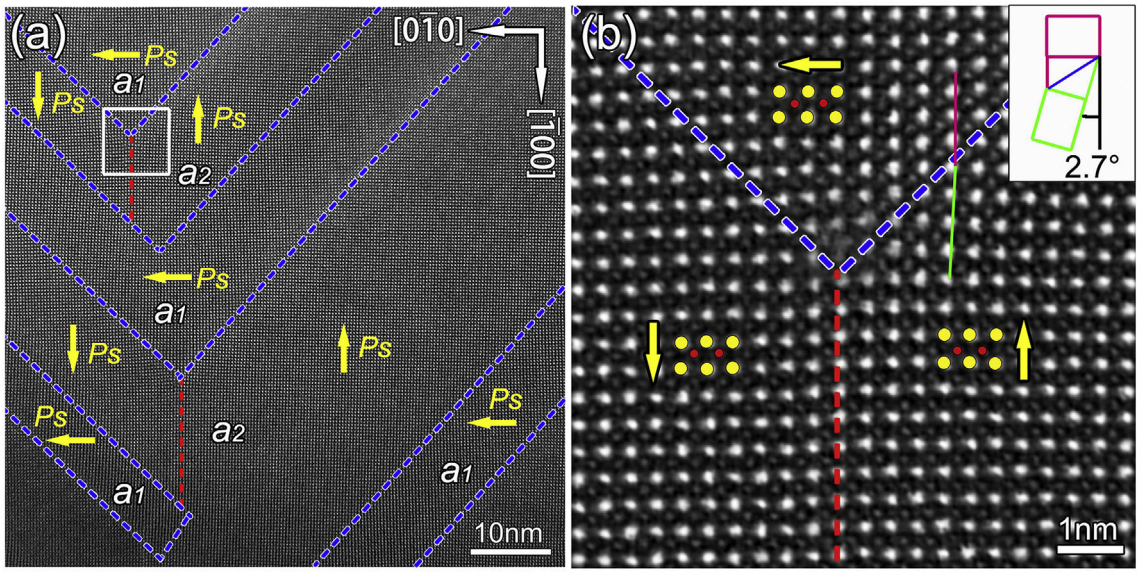

Fig. 5. (a) A high-resolution HAADF-STEM image showing the intersection of a_1/a_2 domains from plan-view observation. Yellow arrows denote the directions of spontaneous polarization (Ps) in each domain. (b) An atomically resolved HAADF-STEM image of the area labeled with a rectangle in (a). The yellow and red circles denote the positions of Pb and Ti atom columns, respectively. The purple and green lines indicate the lattice misorientation on two sides of 90° a_1/a_2 domain wall. The inset is a schematic showing the lattice rotation angle around the 90° domain wall. Yellow arrows denote reversed Ti atom displacement directions. The blue dashed lines indicate 90° domain walls while red dashed lines indicate 180° domain walls in both (a) and (b). (For interpretation of the references to colour in this figure legend, the reader is referred to the web version of this article.)

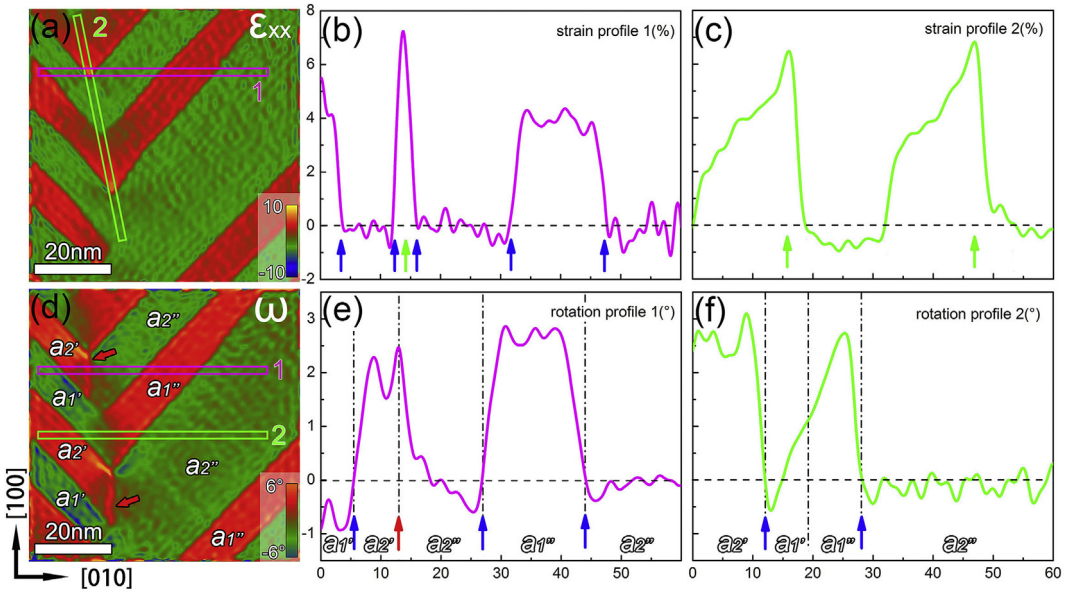

Fig. 6. GPA analysis of Fig. 5(a). (a–c) In-plane strain (ε_{xx}) map and corresponding line profiles of areas labeled 1 and 2 in (a). (d–f) Lattice rotation (ω) map and corresponding line profiles of areas labeled 1 and 2 in (d). Note the inhomogeneous distribution of the strains and lattice rotations at domain walls. Blue arrows in (b), (e) and (f) denote the abrupt changes of lattice strain (rotation) at 90° a_1/a_2 domain walls. Green arrows in (b) and (c) denote the large strain at the peaks of the intersections of a_1/a_2 domains. Red arrow in (d) and (e) denotes the rotation maximal point at 180° domain wall. To facilitate analysis, a_1/a_2 domains with one orientation in (d–f) are named as a_1' and a_2', with the other orientation, named as a_1'' and a_2'', respectively. (For interpretation of the references to colour in this figure legend, the reader is referred to the web version of this article.)

inhomogeneous. If in-plane strain in a_2 domain is set to be zero, then it increases to 4% in a_1 domain due to the different *c*-axis orientations of a_1 and a_2 domains. In this way, 90° a_1/a_2 domain walls can be obviously resolved by locating the dividing boundaries between the red and green areas which can be intuitively seen. Combing with the line profiles, the strain shows local maximum of about 7% around the vertices of the vertex domains, as marked by green arrows in Fig. 6(b) and (c). In this image, blue arrows denote the positions of domain walls across the scanning routes. Similarly, lattice rotation (ω) map (Fig. 6(d)) and line profiles (Fig. 6(e–f)) show the same tendency of a_1/a_2 domain distribution. In Fig. 6(d), if the lattice rotation angle of a_2 domains is set to be 0°, then the angle will be 3° for a_1 domains. As a result, it is also easy to tell a_1 domains from a_2 domains by simply introducing lattice rotation mapping. More importantly, besides 90° a_1/a_2 domain walls, 180° domain walls are visible in rotation angle map, which are pointed out by red arrows in Fig. 6(d). We can also find the abrupt change around 180° domain walls by specifying the peak denoted by red arrow in Fig. 6(e), which is a point at route 1 corresponding to 180° domain wall in Fig. 6(d). To facilitate analysis, the a_1/a_2 domains with domain walls along [$\bar{1}$ 10] are named as a_1' and a_2'; while the a_1/a_2 domains with domain walls along [$\bar{1}$ $\bar{1}$ 0] are a_1'' and a_2'' in Fig. 6(d–f), respectively. From Fig. 6(d), it is easy to understand that a small rotation angle of about 3° exists between a_1' and a_2' domains or a_1'' and a_2'' domains because 90° domain walls lie there. In comparison with an abrupt jump of rotation angle from 0° for a_2' to around 3° for a_2'' domains, the rotation angle changes gradually from a_1' to a_1'' domains, probably showing some relevance with the absence of 180° domain wall. It is noted that 180° domain walls can be identified between a_2' and a_2'' domains, while no 180° domain walls exist between a_1' and a_1'' domains. It was previously reported that there is a specific relationship between lattice rotation and *Ps* at 180° domain walls [30]. Based on Fig. 6(d), the spontaneous polarization (*Ps*) directions on two sides of the 180° domain wall can be identified for a large area and the result agrees well with the denotations in Fig. 5(a).

4. Discussion

The relationship between periodic domain width and film thickness had been theoretically studied before. According to Kittel's law, stripe-domain width in thin film ferromagnetics is predominantly determined by the bulk domain energy E_d, the domain-wall energy E_w, and the film thickness d [14]. This law was further extended for all ferroics and developed to the universal square root dependence of $W \propto d^{1/2}$ [14,15], where W is the width of the periodic domain structure and d is film thickness. Later, the theory was extended to ferroelectric and ferroelastic epitaxial tetragonal films with *a*/*c* and *a*/*a* domain structures under different strain states [16]. In contrast to numerous experimental studies on the evolution of *a*/*c* domain width versus film thickness [7,8,27], experimental observation on a_1/a_2 domain structure is rare, although in-plane ferroelectric nanodomains in strained thin films were discussed by means of atomic force and piezoresponse force microscopies [26]. In the present study, the dependence of W with d for the a_1/a_2 domain is systemically investigated. Kittel's law is marked by black dashed line in Fig. 4 while our experiment data are very consistent with it. Therefore our experimental results about the connection between width of a_1/a_2 domain and film thickness agree well with the theoretical prediction and strongly support these theories.

In addition, previous theoretical work proposed that the shear strain between a_1 and a_2 domains is similar to the strain which may be released by the formation of interfacial defects like continuously distributed screw dislocations, Somigliana dislocation quadrupoles or disinclination quadrupoles [16,25]. From TEM images in Figs. 1 and 3, dislocations are not observed at the interfaces. It is proposed that the shear strain may be accommodated by the lattice rotation between a_1 and a_2 domains as observed in Figs. 2(d) and 6(d). The lattice rotations in diffraction (Fig. 2(d)) and in high-resolution HAADF-STEM (Fig. 6(d)) are believed to reflect the characteristics of ferroelastic domain wall in tetragonal ferroelectrics. It is pointed out earlier that the angle measured from split spots near (011) reflection in Fig. 2(d) is about 1.5°. Similar result has been observed before and is attributed to the in-plane tilting of

the a_1/a_2 domain highly restricted by the binding force of the substrate [20]. In our work, the small angle is considered to be caused by the different interplanar spacing of a_1 and a_2 domains along [010] direction. It is given by Ref. [31].

$$\theta = 45^\circ - \arctan(a/c) \quad (1)$$

Calculated with the lattice constant of bulk PTO, the angle should be 1.8° (in agreement with the experimental value of 1.5°). For the lattice rotation about 3.6° on two sides of 90° a_1/a_2 domain wall (similar to a/c domain wall), it can be seen in the plan-view observations as shown in Figs. 5(b) and 6(d). But the angle measured here is about 2.7° which is smaller than 3.6° for a fully relaxed PTO because the substrate constraint may reduce the tetragonality of the film. Nevertheless, the lattice rotation angle of about 3° between a_1' *and* a_1'' domains or a_2' and a_2'' domains is unanticipated. It is especially perplexing about the rotation misfit between a_1' and a_1'' domains because the *Ps* directions of a_1' *and* a_1'' domains are both parallel to the [0$\bar{1}$ 0] direction and no domain walls exist there. We speculate it is the consequence of substrate clamping effect due to the coherent growth of the PTO film on the substrate in our experiment. According to the characteristic of 90° domain wall, a rotation angle of about 3° exists between a_1' and a_2' domains as expected. Assuming there is no lattice rotation misfit between a_1' and a_1'' domains, the a_2' and a_2'' domains on two sides of 180° domain wall will bear a rotation angle as high as about 6°. It will induce a huge shear strain between the film and substrate, in which case the film cannot be stabilized. The area where two 90° a_1/a_2 domain wall and one 180° domain wall form a three-way intersection, as shown in Fig. 5(b), is called a vertex domain which shows a little difference with vortex studied before [12,32–36]. Unlike the similar structures induced by insulation boundary conditions in other ferroelectrics [11,32], the formation of the threefold vertex domains here with the specific domain configuration and lattice rotation may mainly result from the substrate constraint. As denoted by green arrows in Fig. 5(b–c), there is a large strain concentration at the core of the vertex domain. It can also been inferred from Fig. 5(b) in which the atomic columns appear blurred at the intersection of the threefold domain walls because the lattice displaces badly and the atoms are not regularly arranged due to the large strain concentration at the core.

In ferroelectric films, the formation of domain configuration is a consequence of minimizing the total energy including electrostatic energy, elastic strain energy and domain wall formation energy which is affected by film thickness, substrate mismatch strain, depolarizing field. To better comprehend the formation of the domain pattern in this experiment, the lattice mismatch between the film and substrate at room temperature can be calculated by the following Equation (hypothesizing PTO film is *c*-domain) [24]:

$$f = \frac{a(\mathrm{GSO}) - a(\mathrm{PTO})}{(a(\mathrm{GSO}) + a(\mathrm{PTO}))/2} \times 100\% \approx 1.8\% \quad (2)$$

Since no misfit dislocations can be found at the interfaces, the large tensile stress supplied by substrate may prefer to be accommodated by the formation of multiple domain structure in PTO films.

According to the phase diagrams for (001)-oriented PTO calculated using phase-field simulations, the in-plane strain at room temperature is calculated to be about 0.33% for the present study (the lattice parameter of PTO is adopted for the cubic phase of free-standing films in calculations) which lies in the a/c region and quite close to the a_1/a_2 region [17]. In addition, the volume fraction of c domain in our experiment is also not the same as that in the simulations. This slight difference may be explained by two reasons. One is that the kinetics of domain formation may play a significant role. For example, Ludwig Feigl et al. reported that the cooling rate during annealing has a strong influence on the domain pattern [8]. It implies that the system may not reach its mechanical equilibrium completely under the cooling rate used here and thus may promote the formation of a_1/a_2 domains. The other is that some hypotheses in simulations do not fully conform to our experiment situation, for instance, the contributions of surface and interface to the free energy should not be ignored and the top surface of film may not be stress free in our experiment. Different thermal expansion coefficients of the film and substrate are also a significant factor which is not taken into consideration. Our result may provide data for the modification of the theoretical calculation to obtain more accurate description of the actual phenomenon. As shown in Fig. 3, the area of each a_1/a_2 or a/c domain structure enlarges with increasing film thickness while the fraction of a_1/a_2 domain remains constant of about 50%. It may imply that the type of domain structures is controlled by misfit strain while the width and distribution are affected by film thickness in our experiment, which is in accordance with theoretical predictions [37].

5. Conclusion

In this study, complex domain configuration consisting of a/c and a_1/a_2 domain structures, especially the details of a_1/a_2 domains, were investigated by TEM analysis on PTO films with various thicknesses grown on $(110)_o$-oriented GSO substrate. Our data provide direct evidence that the a_1/a_2 domain periods are proportional to the square root of the film thicknesses, which is in good agreement with theoretical predictions. The misfit strain of this system is mainly relaxed by formation of multiple domain patterns. The domain walls have the rotation characteristic of 90° ferroelastic domain wall. The rotation angle between a_1 and a_2 domains decreases a little rendered by substrate restrictions. Threefold vertex domains composed of two 90° and one 180° domain walls have been observed near the intersection of a_1/a_2 domain structures with different domain wall orientations. Strain mapping indicates that the strains concentrate on domain walls. It is proposed that suitable substrates and deposition parameters such as cooling rate can be used to modulate the domain patterns in ferroelectric films.

Acknowledgements

This work is supported by the National Natural Science Foundation of China (No. 51571197, 51231007, 51501194 and 51671194), National Basic Research Program of China (2014CB921002), and the Key Research Program of Frontier Sciences CAS (QYZDJ-SSW-JSC010). Y. L. T. acknowledges the IMR SYNL-T.S. Kê Research Fellowship and the Youth Innovation Promotion Association CAS (No. 2016177). We are grateful to Mr. B. Wu and Mr. L.X. Yang of this lab for their technical support on the Titan platform of G^2 60–300 kV aberration-corrected scanning transmission electron microscope.

References

[1] J.F. Scott, C.A. Paz de Araujo, Ferroelectric memories, Science 246 (1989) 1400–1405.
[2] J.F. Scott, Applications of modern ferroelectrics, Science 315 (2007) 954–959.
[3] S.K. Choi, S.H. Ahn, W.W. Jung, J.C. Park, S.A. Song, C.B. Lim, Y. Cho, Observation of [110] surface band within {101} a-domain of heteroepitaxial PbTiO3 thin film fabricated by hydrothermal epitaxy, Appl. Phys. Lett. 88 (2006) 052901.
[4] H. Nakaki, Y.K. Kim, S. Yokoyama, R. Ikariyama, H. Funakubo, S.K. Streiffer, K. Nishida, K. Saito, A. Gruverman, Experimental evidence of strain relaxed domain structure in (100)/(001)-oriented epitaxial lead titanate thick films grown by metal organic chemical vapor deposition, J. Appl. Phys. 104 (2008) 064121.
[5] S.P. Alpay, A.L. Roytburd, Thermodynamics of polydomain heterostructures. III. Domain stability map, J. Appl. Phys. 83 (1998) 4714–4723.

[6] A.L. Roytburd, S.P. Alpay, L.A. Bendersky, V. Nagarajan, R. Ramesh, Three-domain architecture of stress-free epitaxial ferroelectric films, J. Appl. Phys. 89 (2001) 553–556.
[7] O. Nesterov, S. Matzen, C. Magen, A.H.G. Vlooswijk, G. Catalan, B. Noheda, Thickness scaling of ferroelastic domains in $PbTiO_3$ films on $DyScO_3$, Appl. Phys. Lett. 103 (2013) 142901.
[8] L. Feigl, P. Yudin, I. Stolichnov, T. Sluka, K. Shapovalov, M. Mtebwa, C.S. Sandu, X.K. Wei, A.K. Tagantsev, N. Setter, Controlled stripes of ultrafine ferroelectric domains, Nat. Commun. 5 (2014).
[9] Q.Y. Qiu, R. Mahjoub, S.P. Alpay, V. Nagarajan, Misfit strain-film thickness phase diagrams and related electromechanical properties of epitaxial ultra-thin lead zirconate titanate films, Acta Mater 58 (2010) 823–835.
[10] Q.Y. Qiu, V. Nagarajan, S.P. Alpay, Film thickness versus misfit strain phase diagrams for epitaxial $PbTiO_3$ ultrathin ferroelectric films, Phys. Rev. B 78 (2008) 064117.
[11] Y.L. Tang, Y.L. Zhu, X.L. Ma, A.Y. Borisevich, A.N. Morozovska, E.A. Eliseev, W.Y. Wang, Y.J. Wang, Y.B. Xu, Z.D. Zhang, S.J. Pennycook, Observation of a periodic array of flux-closure quadrants in strained ferroelectric $PbTiO_3$ films, Science 348 (2015) 547–551.
[12] C.L. Jia, K.W. Urban, M. Alexe, D. Hesse, I. Vrejoiu, Direct observation of continuous electric dipole rotation in flux-closure domains in ferroelectric Pb(Zr,Ti)O-3, Science 331 (2011) 1420–1423.
[13] Y.L. Li, S.Y. Hu, Z.K. Liu, L.Q. Chen, Phase-field model of domain structures in ferroelectric thin films, Appl. Phys. Lett. 78 (2001) 3878–3880.
[14] C. Kittel, Theory of the structure of ferromagnetic domains in films and small particles, Phys. Rev. 70 (1946) 965–971.
[15] A.L. Roitburd, Equilibrium structure of epitaxial layers, Phys. Stat. Sol. (a) 37 (1976) 329–339.
[16] N.A. Pertsev, A.G. Zembilgotov, Energetics and geometry of 90° domain structure in epitaxial ferroelectric and ferroelastic films, J. Appl. Phys. 78 (1995) 6170–6180.
[17] V.G. Koukhar, N.A. Pertsev, R. Waser, Thermodynamic theory of epitaxial ferroelectric thin films with dense domain structures, Phys. Rev. B 64 (2001) 214103.
[18] V.G. Kukhar, N.A. Pertsev, H. Kohlstedt, R. Waser, Polarization states of polydomain epitaxial $Pb(Zr_{1-x}Ti_x)O_3$ thin films and their dielectric properties, Phys. Rev. B 73 (2006) 214103.
[19] Y.L. Li, S.Y. Hu, Z.K. Liu, L.Q. Chen, Effect of substrate constraint on the stability and evolution of ferroelectric domain structures in thin films, Acta Mater 50 (2002) 395–411.
[20] K.S. Lee, J.H. Choi, J.Y. Lee, S. Baik, Domain formation in epitaxial $Pb(Zr,Ti)O_3$ thin films, J. Appl. Phys. 90 (2001) 4095–4102.
[21] F. Borodavka, I. Gregora, A. Bartasyte, S. Margueron, V. Plausinaitiene, A. Abrutis, J. Hlinka, Ferroelectric nanodomains in epitaxial $PbTiO_3$ films grown on $SmScO_3$ and $TbScO_3$ substrates, J. Appl. Phys. 113 (2013) 187216.
[22] S. Yasui, Y. Ehara, S. Utsugi, M. Nakajima, H. Funakubo, A. Gruverman, Complex domain structure in relaxed $PbTiO_3$ thick films grown on (100) $cSrRuO_3$//(100)$SrTiO_3$ substrates, J. Appl. Phys. 112 (2012) 052001.
[23] S. Stemmer, S.K. Streiffer, F. Ernst, M. Ruhle, Atomistic structure of 90° domain walls in ferroelectric $PbTiO_3$ thin films, Philo. Mag 71 (1995) 713–724.
[24] S. Stemmer, S.K. Streiffer, F. Ernst, M. Ruhle, W.Y. Hsu, R. Raj, Domain configuration in ferroelectric $PbTiO_3$ thin films: the influence of substrate and film thickness, Solid State Ionics 75 (1995) 43–48.
[25] A.E. Romanov, W. Pompe, J.S. Speck, Theory of microstructure and mechanics of the...$a_1/a_2/a_1/a_2$... domain pattern in epitaxial ferroelectric and ferroelastic films, J. Appl. Phys. 79 (1996) 4037–4049.
[26] S. Matzen, O. Nesterov, G. Rispens, J.A. Heuver, M. Biegalski, H.M. Christen, B. Noheda, Super switching and control of in-plane ferroelectric nanodomains in strained thin films, Nat. Commun. 5 (2014).
[27] A.H.G. Vlooswijk, B. Noheda, G. Catalan, A. Janssens, B. Barcones, G. Rijnders, D.H.A. Blank, S. Venkatesan, B. Kooi, J.T.M. de Hosson, Smallest 90° domains in epitaxial ferroelectric films, Appl. Phys. Lett. 91 (2007) 112901.
[28] G. Catalan, A. Lubk, A.H.G. Vlooswijk, E. Snoeck, C. Magen, A. Janssens, G. Rispens, G. Rijnders, D.H.A. Blank, B. Noheda, Flexoelectric rotation of polarization in ferroelectric thin films, Nat. Mat. 10 (2011) 963–967.
[29] G. Shirane, S. Hoshino, On the phase transition in lead titanate, J. Phys. Soc. Jpn. 6 (1951) 265–270.
[30] Y.L. Tang, Y.L. Zhu, X.L. Ma, On the benefit of aberration-corrected HAADF-STEM for strain determination and its application to tailoring ferroelectric domain patterns, Ultramicroscopy 160 (2016) 57–63.
[31] J.S. Speck, A.C. Daykin, A. Seifert, A.E. Romanov, W. Pompe, Domain configurations due to multiple misfit relaxation mechanisms in epitaxial ferroelectric thin films. III. Interfacial defects and domain misorientations, J. Appl. Phys. 78 (1995) 1696–1706.
[32] C.T. Nelson, B. Winchester, Y. Zhang, S.-J. Kim, A. Melville, C. Adamo, C.M. Folkman, S.H. Baek, C.B. Eom, D.G. Schlom, L.Q. Chen, X. Pan, Spontaneous vortex nanodomain arrays at ferroelectric heterointerfaces, Nano Lett. 11 (2011) 828–834.
[33] D.J. Srolovitz, J.F. Scott, Clock-model description of incommensurate ferroelectric films and of nematic-liquid-crystal films, Phys. Rev. B 34 (1986) 1815–1819.
[34] J.M. Gregg, Exotic domain states in ferroelectrics: searching for vortices and skyrmions, Ferroelectrics 433 (2012) 74–87.
[35] B. Lee, S.M. Nakhmanson, O. Heinonen, Strain induced vortex-to-uniform polarization transitions in soft-ferroelectric nanoparticles, Appl. Phys. Lett. 104 (2014) 262906.
[36] J. Mangeri, Y. Espinal, A. Jokisaari, S. Pamir Alpay, S. Nakhmanson, O. Heinonen, Topological phase transformations and intrinsic size effects in ferroelectric nanoparticles, Nanoscale 9 (2017) 1616–1624.
[37] A.L. Roytburd, Thermodynamics of polydomain heterostructures. II. Effect of microstresses, J. Appl. Phys. 83 (1998) 239–245.